

Figure 1. (a) Track and radar coverage of Hurricane Charley from 0800 UTC 13 August to 0105 UTC 14 August 2004. Range rings indicate maximum Doppler coverage (174 km) for Key West (KBYX) and Tampa (KTBW) WSR-88D radars. Colors indicate NHC best track Saffir-Simpson scale intensity. (b)–(g) Constant altitude PPI reflectivity at 2 km at six different analysis times.

Doppler velocities in a TC centered cylindrical coordinate system [Lee et al., 1999]. The TC center is defined as a point that yields the maximum circulation enclosed by the radius of maximum wind deduced from the GBVTD-simplex algorithm [Lee and Marks, 2000]. Since Doppler velocities are azimuthally periodic on rings around this TC center, a Fourier analysis can decompose the structure of the radar winds at each radius via a circular wind model. The three-dimensional TC circulation can be deduced from the Fourier coefficients to provide the along beam (in the direction of the radar and TC center) component of the mean environmental wind, axisymmetric (azimuthal mean) tangential and radial winds, and asymmetric tangential winds. Unresolved asymmetric radial winds, which may be large in a landfall situation due to an enhanced surface roughness gradient, and the cross-beam (normal to radar-TC center direction) component of the mean wind are aliased into the resolved quantities. In particular, the unresolved azimuthal wave number two radial wind may bias the retrieved symmetric primary (tangential) and secondary (transverse) circulations (details are discussed in Lee et al. [1999]). Harasti et al. [2004] demonstrated application of the GBVTD-derived wind fields to nowcasting of land-falling TCs. Evolution and structures of intense landfalling TCs in the Indian Ocean (e.g., TC Dina) and northwestern Pacific (e.g., Typhoon Nari) have been deduced from GBVTD [Roux et al., 2004] and EGBVTD [Liou et al., 2006], respectively. The grid spacing for the GBVTD analyses of Charley is 1 km in both radial and vertical directions, adequate to resolve the axisymmetric kinematic structures. Dynamic quantities, such as the vertical velocities, vorticity, angular momentum and pressure deficits, can be computed from the GBVTD-derived axisymmetric circulations [Lee et al., 2000].

3. Results

[7] The low-level reflectivity structures (dBZ, 2 km constant altitude PPI) of Charley at six time periods (from 1100 UTC 13 August 2004 to 0000 UTC 14 August 2004) are illustrated in Figures 1b–g. Charley possessed a distinct eyewall accompanied by several rainbands spiraling out

from the eyewall at 1100 UTC (Figure 1b). The reflectivity of the rainbands weakened at 1400 UTC (Figure 1c) but re-intensified at 1700 UTC to form a double eyewall (Figure 1d). The size of the eye continued to contract until Charley made landfall at 2000 UTC (Figure 1e). The eye filled with precipitation as Charley moved inland and gradually lost its organization (Figures 1f and 1g).

[8] The evolution of Charley is illustrated using the GBVTD-derived radial profiles of the axisymmetric tangential winds at $z = 3$ km at five times; 1100, 1400, 1700, 2000, and 2300 UTC (Figure 2). Charley's intensity inferred from the axisymmetric tangential winds peaked around 1700 UTC with a magnitude of 53 m s^{-1} and maintained its intensity until its landfall around 2000 UTC. After landfall, the axisymmetric tangential wind speed decreased rapidly to 35 m s^{-1} at 2300 UTC. During the intensifying phase, Charley's radius of maximum wind fell from 13 km to 8 km between 1400 and 2000 UTC; Charley's inner core then expanded into a broad and flat pattern at 2300 UTC. From the distribution of the axisymmetric tangential wind profile (Figure 2a), the integrated kinetic energy of Charley (proportional to the area beneath each curve) peaked around 1700 UTC.

[9] The vertical vorticity patterns outside the eyewall are quite similar among all five analyses with a magnitude 0.001 s^{-1} . However, an intriguing evolution of vertical vorticity in the core region is apparent. A ring vorticity profile (vertical vorticity peaked near the radius of maximum wind so that the radial vorticity gradient changes sign), which satisfies the necessary condition for a combined barotropic-baroclinic instability [Montgomery and Shapiro, 1995], existed at 1100 UTC and intensified until 1400 UTC with a peak vorticity of 0.011 s^{-1} at $R = 5 \text{ km}$. The ring vorticity profile of Charley evolved into a monopole pattern (vertical vorticity peaked at the TC center) at 1700 UTC with a peak vorticity exceeding 0.02 s^{-1} at $R = 3 \text{ km}$, the inner most radius of the analyses. Previous studies using theoretical arguments and barotropic numerical models [Schubert et al., 1999], laboratory tank experiments [Montgomery et al., 2002] and composite aircraft in situ data [Mallen et al., 2005], have all emphasized the importance of the axisymmetric vorticity profile on hurricane

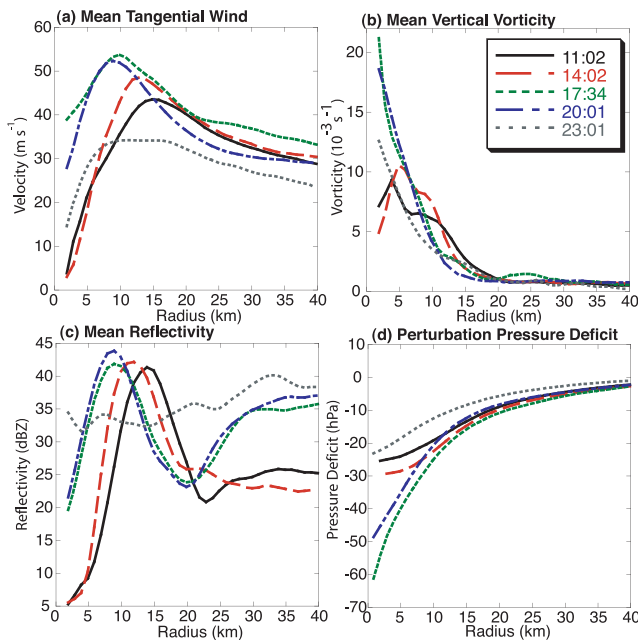


Figure 2. Radial profiles at $z = 3$ km from five analysis times (1102, 1402, 1734, 2001, and 2301 UTC). Different line styles/colors represent analysis times; (a) mean tangential wind (m s^{-1}), (b) mean vertical vorticity (10^{-3} s^{-1}), (c) mean reflectivity (dBZ), and (d) perturbation pressure deficit (hPa) assuming zero at 60 km radius. Analysis domain extends to 60 km radius, but results out to 40 km are shown for clarity. Hurricane eyewall is area of high reflectivity and wind speed near 10 km radius.

evolution and intensity. The high temporal and spatial resolution of this analysis provides the first observational evidence of the transition of the axisymmetric vorticity profile from an unstable ring to a more stable monopole configuration after the vortex reached peak intensity, which has been previously suggested from composite aircraft in situ data [Kossin and Eastin, 2001]. In this case, a forecaster may have been able to use knowledge of the vorticity profile transition to nowcast that Charley might have reached its peak intensity and further deepening was unlikely.

[10] The shrinking of the radius of maximum wind was concurrent with the contraction of the eyewall. The observed weak reflectivity and deduced downdraft on both sides of the eyewall were consistent with a forced response of a balanced vortex to the latent heat release associated with eyewall convection [Eliassen, 1952; Shapiro and Willoughby, 1982]. Although the eyewall reflectivity slightly increased between 1400 and 2000 UTC, the dramatic increase of the mean reflectivity by 15 dBZ beyond $R = 20$ km was striking. This indicates the formation of a secondary eyewall (Figures 1c and 1d), but there was no secondary wind maximum typically associated with an outer eyewall or concentric rainbands in Charley. We speculate there may be an asymmetric secondary wind maximum and/or a potential lag between the reflectivity and velocity fields during the eyewall replacement cycle. This process might have been disrupted by landfall, preventing the completion of the secondary eyewall formation,

although it is notable that the outer reflectivity maximum was enhanced over land, possibly due to increased surface friction and convergence. After Charley's landfall, the inner eyewall collapsed and the peak reflectivity shifted to $R = 32$ km accompanied by a broad radial rainfall distribution.

[11] Rapid intensification of Charley can be further illustrated using the perturbation pressure deficits in these five time periods (Figure 2d). Since the radar does not directly measure pressure, the symmetric radial momentum equation was integrated inward using the GBVTD derived winds, assuming the total pressure at $R = 60$ km remained steady. Charley's central pressure dropped 33 hPa from 1400 to 1700 UTC, filled 13 hPa between 1700 and 2000 UTC, then filled another 25 hPa after its landfall at 2300 UTC. The 11 hPa hr^{-1} pressure drop between 1400 to 1700 UTC in Charley exceeded the 9.9 hPa hr^{-1} in Hurricane Wilma (2005), the most intense Atlantic hurricane on record [Pasch et al., 2006]. Note that the two dropsondes released at 1522 and 1957 UTC [Franklin et al., 2006] completely missed the deepening of central pressure from 1400 to 1700 UTC and the filling of central pressure from 1700 to 2000 UTC based on the radar analysis. With the Doppler radar data, the pressure changes can be monitored at a much higher frequency than those can be provided by the aircraft reconnaissance and dropsonde observations.

[12] Vertical cross sections of the axisymmetric structure of Charley are illustrated in Figure 3 at 1400 UTC. In Figure 3a the tangential wind speed (solid lines) and reflectivity (color scale) indicate that the radii of the maximum reflectivity and tangential wind are 11 km and 13 km, respectively, indicating a tight vortex. Both the eyewall reflectivity and axisymmetric tangential wind field were upright below 6 km and tilted outward above. The maximum axisymmetric tangential wind at $z = 1$ km exceeded 50 m s^{-1} and the wind speeds decreased with height. Vertical velocity was calculated from the radial divergence field using the kinematic method [Armijo, 1969], and the derived secondary, or meridional, circulation (vectors, Figure 3b) shows an inflow layer below 3 km that turned into updraft beneath the eyewall [Marks et al., 1992; Lee et al., 1994; Lee et al., 2000]. Eyewall updrafts reached 13 km altitude (Figure 3b). The eyewall reflectivity structure suggests that the updraft and outflow continue above 14 km altitude, beyond the analysis domain. The secondary circulation in Figure 3b shows an inflow layer beneath the anvil outflow, centered at $z = 10$ km outside the eyewall, converged with the outflow from the eyewall and turned into a downdraft. This is consistent with the downward and inward kink evident in the reflectivity (e.g., $R = 20$ km and $z = 8$ km). The inflow layer below the anvil has been deduced in Hurricane Gloria (1985) [Lee et al., 1994] and numerical simulations [e.g., Rotunno and Emanuel, 1987]. However, the significance of this feature has yet to be explored. A weaker updraft located at $R = 35$ km appears to precede the enhancement of reflectivity at this radius later in the storm's evolution (see Figure 2c). Since the secondary circulation was derived independently from the reflectivity, the good correlations between them suggest that the secondary circulation is physically plausible.

[13] The pressure deficits (Figure 3c) exhibited a dome-shaped pattern with the horizontal pressure gradient

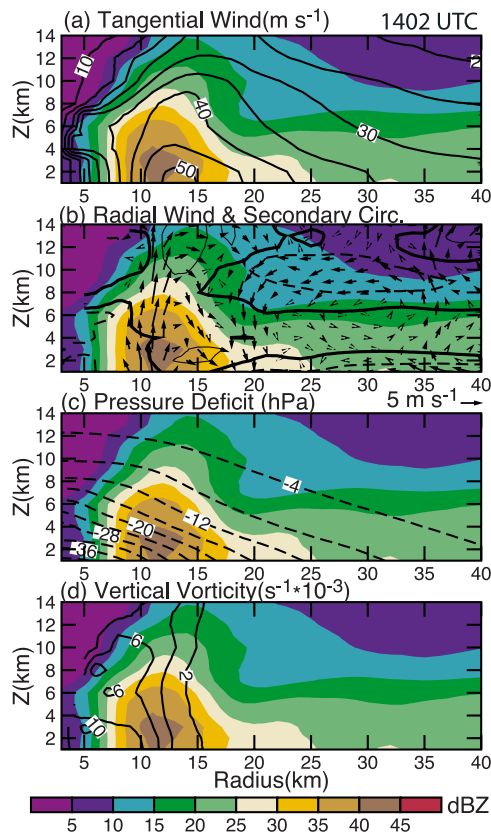


Figure 3. Radius-height cross-section of the azimuthal mean structure at 1402 UTC. Color represents reflectivity in dBZ; contours are (a) mean tangential wind (m s^{-1}), (b) mean radial wind (m s^{-1}), (c) perturbation pressure deficit (hPa) assuming zero at 60 km radius, and (d) mean vertical velocity ($\text{s}^{-1} \times 10^{-3}$). Vectors in Figure 3b indicate mean secondary circulation. Analysis domain extends to 60 km radius, but results out to 40 km are shown for clarity.

decreasing with height, in agreement with other tropical cyclone observations and modeling studies [e.g., Lee et al., 2000; Rotunno and Emanuel, 1987]. The central pressure deficit at $z = 1$ km was 41 hPa from 60 km radius. The axisymmetric vorticity (Figure 2d) shows a maximum of 0.01 s^{-1} located at $R = 5$ km, which is inside the radius of maximum wind of 13 km, indicating a mature storm satisfying the condition for barotropic instability as mentioned previously. The vorticity gradient is concentrated inside the eyewall where the radial gradient of the tangential wind is maximized.

4. Summary and Future Work

[14] This study presents a preliminary analysis of Hurricane Charley's kinematic and dynamic structures before and after its Florida landfall using the coastal WSR-88D data and the GBVTD technique. The GBVTD-derived tangential wind, vorticity and perturbation pressure deficit reveal rapid intensification of Charley before its landfall. The rapid intensification of Charley was accompanied by an eyewall contraction. The WSR-88D data documented the 11 hPa hr^{-1} drop of central pressure over a three-hour

period that ranks Charley among the most rapidly intensifying hurricanes in the Atlantic basin. Charley's radial vorticity profile evolved from unstable to stable after it reached its peak intensity.

[15] As a logical next step, we propose to (1) analyze WSR-88D data to document the evolution of Hurricane Charley in six-minute intervals over the 18 hour period, (2) deduce the asymmetric structure of Charley, (3) compare the pressure derived from the Doppler radar data to those measured by dropsondes released by reconnaissance aircraft, and (4) compare results with high resolution numerical models.

[16] Acknowledgments. We would like to thank Paul Harasti for his comments on the analysis. Internal reviews provided by D. Parsons, T. Weckwerth, and S. Ellis greatly improved this manuscript. We appreciate the comments and suggestions provided by two anonymous reviewers that significantly improve the content and clarity of this manuscript. We would also like to acknowledge the National Weather Service and National Climatic Data Center for collecting and archiving the NEXRAD Level II data used in this study. The National Center for Atmospheric Research is sponsored by the National Science Foundation.

References

- Armijo, L. (1969), A theory for the determination of wind and precipitation velocities with Doppler radars, *J. Atmos. Sci.*, 26, 570–573.
- Dvorak, V. (1975), Tropical cyclone intensity analysis and forecasting from satellite imagery, *Mon. Weather Rev.*, 103, 420–430.
- Dvorak, V. (1984), Tropical cyclone intensity analysis using satellite data, NOAA Tech. Rep. NESDIS 11, 47 pp., Natl. Oceanic and Atmos. Admin., U. S. Dep. Of Comm., Washington, D. C.
- Eliassen, A. (1952), Slow thermally or frictionally controlled meridional circulation in a circular vortex, *Astrophys. Norv.*, 5, 19–30.
- Franklin, J. L., R. J. Pasch, L. A. Avila, J. L. Beven, M. B. Lawrence, S. R. Stewart, and E. S. Blake (2006), Annual summary, Atlantic hurricane season of 2004, *Mon. Weather Rev.*, 134, 981–1025.
- Harasti, P. R., C. J. McArdie, P. P. Dodge, W.-C. Lee, J. Tuttle, S. T. Murillo, and F. D. Marks Jr. (2004), Real-time implementation of single-Doppler radar analysis methods for tropical cyclones: Algorithm improvements and use with WSR-88D display data, *Weather Forecast.*, 19, 219–239.
- Kossin, J. P., and M. D. Eastin (2001), Two distinct regimes in the kinematic and thermodynamic structure of the hurricane eye and eyewall, *J. Atmos. Sci.*, 58, 1079–1090.
- Lee, W.-C., and F. D. Marks Jr. (2000), Tropical cyclone kinematic structure retrieved from single Doppler radar observations. part II: The GBVTD-simplex center finding algorithm, *Mon. Weather Rev.*, 128, 1925–1936.
- Lee, W.-C., F. D. Marks, and R. E. Carbone (1994), Velocity track display: A technique to extract real-time tropical cyclone circulations using a single Doppler radar, *J. Atmos. Oceanic Technol.*, 11, 337–356.
- Lee, W.-C., J.-D. Jou, P.-L. Chang, and S.-M. Deng (1999), Tropical cyclone kinematic structure retrieved from single Doppler radar observations. part I: Interpretation of Doppler velocity patterns and the GBVTD technique, *Mon. Weather Rev.*, 127, 2419–2439.
- Lee, W.-C., J.-D. Jou, P.-L. Chang, and F. D. Marks (2000), Tropical cyclone kinematic structure retrieved from single-Doppler radar observations. part III: Evolution and structure of Typhoon Alex (1987), *Mon. Weather Rev.*, 128, 3892–1901.
- Liou, Y.-C., T.-C. C. Wang, W.-C. Lee, and Y.-J. Chang (2006), The retrieval of asymmetric tropical cyclone structures using Doppler radar simulations and observations with the extended GBVTD technique, *Mon. Weather Rev.*, 134, 1140–1160.
- Mallen, K., M. T. Montgomery, and B. Wang (2005), Reexamining the near-core radial structure of the tropical cyclone primary circulation: implications for vortex resiliency, *J. Atmos. Sci.*, 62, 408–425.
- Marks, F. D., R. A. Houze, and J. Gamache (1992), Dual-aircraft investigation of the inner core of Hurricane Norbert. part I: Kinematic structure, *J. Atmos. Sci.*, 49, 919–942.
- Mayfield, M., L. Avila, and E. N. Rappaport (1994), Annual summaries: Atlantic hurricane season of 1992, *Mon. Weather Rev.*, 122, 517–538.
- Montgomery, M. T., and L. J. Shapiro (1995), Generalized Charney-Stern and Fjortoft theorems for rapidly rotating vortices, *J. Atmos. Sci.*, 52, 1829–1833.
- Montgomery, M. T., V. A. Vladimirov, and P. V. Denissenko (2002), An experimental study on hurricane mesovortices, *J. Fluid. Mech.*, 471, 1–32.

- Pasch, R. J., E. S. Blake, H. D. Cobb, and D. P. Roberts (2006), Hurricane Wilma Tropical Cyclone Report, Natl. Hurricane Cent., Miami, Fla.
- Pielke, R. A., Jr., and C. W. Landsea (1998), Normalized hurricane damages in the United States: 1925-1995, *Weather Forecast.*, 13, 621-631.
- Rotunno, R., and K. Emanuel (1987), An air-sea interaction theory for tropical cyclones. part II: Evolutionary study using a non-hydrostatic axisymmetric numerical model, *J. Atmos. Sci.*, 44, 542-561.
- Roux, F., F. Chane-Ming, A. Lasserre-Bigorry, and O. Nuissier (2004), Structure and evolution of intense tropical cyclone Dina near La Réunion on 22 January 2002: GB-EVTD analysis of single Doppler radar observations, *J. Atmos. Oceanic Technol.*, 21, 1501-1518.
- Schubert, W. H., M. T. Montgomery, R. K. Taft, T. A. Guinn, S. R. Fulton, J. P. Kossin, and J. P. Edwards (1999), Polygonal eyewalls, asymmetric eye contraction, and potential vorticity mixing in hurricanes, *J. Atmos. Sci.*, 56, 1197-1223.
- Shapiro, L. J., and H. E. Willoughby (1982), The response of balanced hurricanes to local sources of heat and momentum, *J. Atmos. Sci.*, 39, 378-394.
- Shay, L. K., G. J. Goni, and P. G. Black (2000), Effects of a warm oceanic feature on Hurricane Opal, *Mon. Weather Rev.*, 128, 1366-1383.
- Willoughby, H. E., and P. G. Black (1996), Hurricane Andrew in Florida: Dynamics of a disaster, *Bull. Am. Meteorol. Soc.*, 77, 543-549.
- M. M. Bell and W.-C. Lee, Earth Observing Laboratory, National Center for Atmospheric Research, Boulder, CO 80307, USA.